96-71

Environment Canada

Water Science and Technology Directorate

Direction générale des sciences et de la technologie, eau

Environnement Canada

The Determination of the Orientations of Fracture Planes in a Weathered Clay Till using Core Samples

By:
Steven M. Harrie, Neil R. Thomson

NWRI Contribution # 96-71

96-71

The Determination of the Orientations of Fracture Planes in a Weathered Clay Till using Core Samples

Steven M. Harris[1]
Neil R. Thomson
Department of Civil Engineering, University of Waterloo
Waterloo, Ontario, Canada, N2L 3G1

Kentner S. Novakowski
Canada Centre for Inland Waters,
867 Lakeshore Road, Burlington, Ontario, Canada, L7R 4A6

Abstract

A method has been developed to determine fracture plane orientations in clay-rich glacial deposits from core samples obtained from inclined borings. In this method, a portion of each core sample is removed to expose vertical and horizontal surfaces which are used to map each identified fracture plane. An analytical geometry technique is used in conjunction with the mapping data to determine the pole to each fracture plane. This fracture pole data can then be presented on a lower hemisphere equal area projection diagram to indicate preferred fracture plane orientations. The utility of the developed method is demonstrated through a detailed analysis of core samples collected from a 10 m^2 site located near Sarnia, Ontario. The data from this investigation indicated the presence of three sets of fracture planes; however, only one of these fracture sets was determined to be statistically significant. The developed method offers an alternative to mapping fracture plane orientations on exposed surfaces.

Submitted to Ground Water, May 1996.

[1] Now at Conestoga-Rovers and Associates Limited 651, Colby Drive, Waterloo, Ontario, Canada, N2V 1C2.

MANAGEMENT PERSPECTIVE

The clay plains distributed throughout North America and northern Europe are widely used as repositories for hazardous wastes. This is because thick sequences of clay offer significant barriers to the transport of groundwater contamination that might emanate from a waste facility. However, at some facilities, wastes are placed in excavations which are capped when filled. This creates a groundwater mound and the potential for leakage of contamination in the shallow subsurface. Most of these clay sequences have been subjected repeated cycles of wetting and drying in the shallow subsurface, creating a horizon of weathered clay pervaded by fractures. Thus, the weathered zone provides for a conduit for groundwater flow from the groundwater mounds and the potential for widespread migration of contamination. The primary features controlling the groundwater flow are the fractures which form through desiccation processes.

This paper presents the results of a drilling study of the St. Joesephs Clay Till in Lambton County, Ontario. The objective was to determine the orientations of the fractures in the weathered zone to estimate the directions of preferential flow. A technique originally developed for orienting fracture planes from rock core was adapted using new planes of reference. The results show that there is some preferential directions of fracture orientation which should define the directions of shallow groundwater flow. It was also found that a bias introduced by the orientation of the inclined boreholes made for a difficult interpretation of the confidence levels of the interpretation. A paper to follow on the hydraulic properties of the fractures will illustrate the usefulness of determining fracture orientations.

Introduction

Surficial clay-rich glacial till deposits are common in North America, particularly in the midwestern plains and regions surrounding the Great Lakes. As water levels have fluctuated seasonally, these clay till deposits have been subjected to physical and geochemical weathering which has resulted in a shallow fractured crust that ranges from 5 m to 6 m in thickness (McKay *et al.*, 1993). Recent findings from studies conducted in the shallow weathered zone of clay till deposits suggest that substantial hydraulic activity occurs. The presence of this hydraulic activity indicates that a significant potential exists for solute migration within this zone. This potential can be enhanced with the occurrence of high hydraulic gradients associated with landfill mounds, ditches and agricultural drainage tiles. In the past, near surface contamination sources such as waste disposal landfills were sited on surficial clay till deposits since the unweathered clay till beneath the weathered zone, if sufficiently thick, would prevent deep ground water contamination. Despite physical evidence of surficial fracturing, the hydraulic conductivity of the weathered zone was considered to be sufficiently low to provide lateral hydraulic containment. Thus, lateral solute migration to surface waterways was perceived as negligible. In light of recent studies conducted in fractured clay tills, the potential for these fractures to provide preferential pathways for lateral as well as vertical contaminant migration within the weathered zone should not be ignored.

The capability to estimate the amount and extent of contaminant migration in a fractured clay till, both vertically and laterally from a source, is limited by the ability to characterize the fracture geometry. Since contaminant migration along fractures is expected to be the dominate transport mechanism through a weathered clay till deposit, a methodology to estimate fracture geometry is required. The characterization of fractures within a clay till deposit are usually conducted at locations of naturally or artificially exposed surfaces. Fracture plane orientations defined by the fracture strike and dip angles, fracture frequency or spacing, and relevant fracture surface characteristics such as roughness or chemical deposits, can be estimated on these exposed surfaces (Bosscher and Connell, 1988). The fracture plane orientation data can be resolved and presented on equal area projection plots (e.g., Vorauer *et al.*, 1986). Fracture frequency is usually presented in terms of the number of fractures per horizontal metre with depth from ground surface (e.g., McKay *et al.*, 1993).

The purpose of this paper is to present the development of a method for determining the orientations of fracture planes from inclined boreholes drilled in a clay till deposit. To demonstrate the utility of this method, a detailed analysis of core samples from a number of inclined borings drilled within a relatively small region of a clay till deposit will be described.

The methodology presented in this paper is similar to that described by Lau (1983) to determine fracture orientations from inclined drilled rock cores. However, due to the external

smearing of the clay soil cores a technique to expose undisturbed surfaces is required. This creates a different set of reference points, and hence a different analytical geometry transformation than presented by Lau (1983).

Description of Study Site

The data in this analysis was collected as part of a larger investigation into the hydraulic properties of the shallow weathered zone of a surficial clay till deposit known as the St. Joseph Till located in southwestern Ontario (Harris *et al.*, 1996). Previous field investigations have been conducted within the weathered zone of this deposit at the Lambton Thermal Generating Station near Courtright, Ontario (Vorauer *et al.*, 1986; and Harding, 1986), and at the Laidlaw Hazardous Waste Management Facility near Sarnia, Ontario (Klint, 1996; McKay *et al.*, 1993; Balfour, 1991; Ruland *et al.*, 1991; and D'Astous et al., 1989). In addition to investigating the hydraulic properties and solute migration processes within the weathered zone, these studies focused on describing the characteristics, frequency, extent and orientation of fractures observed in trench excavations and some core samples.

The weathered fractures within this deposit are believed to be formed by dessication and/or freezing mechanisms (Klint, 1996). In general, from ground surface to a depth of ~3.5 m, this clay till deposit is extremely fractured and oxidized, and is reddish-brown in colour with an increasingly darker hue with depth. Fracture surfaces over ~3.5 m depth are characterized by red oxidation staining with intermittent black and grey precipitate coatings. Fractures have been observed at spacings of 1 cm to 10 cm with a primarily vertical to sub-vertical orientation although there is a frequent occurrence of horizontal to sub-horizontal oriented fractures. Between the depths of ~3.5 m and ~5 m, the clay till gradually changes from a brown to a grey colour with spacings ranging from 0.5 m to 2 m.

Trench excavations were conducted at the Laidlaw Hazardous Waste Management Facility (D'Astous *et al.*, 1989; and Ruland *et al.*, 1986) to determine fracture orientations to a depth of ~ 6.0 m. The trenches were excavated in a manner which left the fracture orientations relatively undisturbed. Although, the fractures displayed a dominant vertical to sub-vertical orientation, no preferred fracture plane strike direction could be identified. McKay *et al.* (1993) used the same techniques to map fractures on vertical and horizontal surfaces of small trench excavations and within the larger landfill excavation. The fracture mapping data collected from the vertical surfaces indicated the presence of two sets of orthogonal fracture planes with preferential orientations in the north-south and east-west directions. However, the alignment of these vertical surfaces was coincident with the two preferential fracture orientations. As a result, there is some question whether the dominance of the two fracture orientations may have been due, in part, to stress relief causing fractures parallel to the excavated face to become more visible. Despite this

short coming, the same preferential orientations were observed in the fracture mapping data collected from some of the horizontal surfaces below a depth of 4.0 m. Although at this depth, the areas sampled by the horizontal surface mapping were too small to confirm this finding. In a recent study at this location by Klint (1996), ~110 m of exposed trench walls along five profiles were mapped primarily over a depth interval from ~3 m to 7 m below ground surface. All of these profiles indicated the predominance of a northeast-southwest and a northwest-southeast fracture orientation. In addition, two of the mapped profiles indicated an east-west preferential fracture orientation.

For the investigation described in this paper, a field site was established ~200 m west of the McKay *et al.* (1993) study site on the Laidlaw property. The study site has a topographic relief of no more than ~0.01 m. Overlying the upper zone of weathered clay till is ~0.4 m of black sand. The site consisted of one vertical and eleven angled piezometers installed within a 10 m^2 area. Figures 1(a) and 1(b) present a plan and cross-section view, respectively, of the layout of the piezometers. The boreholes were drilled at inclination angles ranging from 35° to 60° from horizontal. The depth of the 12 piezometers ranged from ~1.8 m to ~5.5 m below ground surface. The piezometers were drilled using a continuous coring technique from which samples having defined orientations were obtained. The details of this methodology along with actual data from the field site are described in this paper.

Field Method

The core samples were obtained using a 7.6 cm inside diameter split-spoon sampling barrel that was advanced using 17.8 cm outside diameter hollow-stem augers. The sampling barrel was inserted into the augers and was attached to the drilling rig by drill rods extending through the centre of the augers. The sampling barrel was set ~15 cm beyond the auger cutting bit. The top of the core was tracked by scoring an orientation line on the exterior of the sampling barrel which was continued in a consistent manner along the drill rods. After positioning the sampling barrel inside the augers, this orientation line was rotated such that it faced vertically upwards. A hand level held in contact with this line was used to ensure that an upward orientation was maintained. The sampling barrel and drill rod assembly were then secured to the drilling rig such that the assembly remained in a constant orientation and did not turn with the augers. As the augers rotated, the sampling barrel, fixed its the upwards orientation, was advanced ahead of the augers in order to cut an undisturbed core sample along the inclination of the borehole. The top of the core corresponded to the orientation line scored on the outside of the sampling barrel. It is estimated that the accuracy of the orientation is ±5°.

After retrieving the sampling barrel the scored orientation line corresponding to the top of the core was transferred to the core ends before separating the sampling barrel. After separating the

sampling barrel, the two marks on the core ends were connected with a continuous line indicating the top of the core. The downhole direction was then indicated on the core before sealing it for transport

The depth interval of each core sample relative to ground surface was measured along the axis of the inclined borehole. Each borehole was completed using a 5 cm diameter piezometer casing that was centered within the borehole annulus using flexible centralizeres. The orientation of the piezometer casing below ground surface was determined using a Tro-Pari borehole directional surveying instrument (Pajari Instruments Ltd., Orillia, Ontario, Canada). By lowering the instrument into the inclined piezometers, measurements of the casing bearing angle β with respect to north and the casing dip angle δ from horizontal were obtained. Since the piezometer casing was centered within the borehole annulus, the measured angles were assumed to be directly transferable to the axis of the borehole. The borehole bearing β_{BH} and borehole dip δ_{BH} angles measured for each of the inclined piezometers are indicated on Figure 1(a). This orientation data was further assumed to represent the axis of the core samples obtained from each respective borehole. In combination with the plunge of the core recorded during sample retrieval, the angles β_{BH} and δ_{BH} provides a means to determine the in-situ orientation of each core sample.

Mapping of the Fracture Plane

The mapping of fractures which were observed to intersect each core sample was conducted on a laboratory bench. To reveal intersected fractures, a quarter of the core sample was carefully cut away by hand to expose vertical and horizontal surfaces. Any smeared clay was diligently chipped away leaving relatively undisturbed surfaces. Figure 2 and 3 provide schematic views of the upper and lower exposed surfaces, respectively, of two example core sections as they would appear during this fracture mapping exercise

For the weathered clay encountered at this site, fractures were identified primarily by the red oxidation staining that created trace lines of the intersected fractures on the exposed surfaces. A discrete fracture plane was identified when two trace lines, continuous across both surfaces met along the axis of the core at a common apex (see Figure 2 and 3). Intersected fracture planes were found to belong to one of two in-situ orientation cases (Case I vertical to sub-vertical orientation, and Case II horizontal to sub-horizontal) as indicated by the shaded three-quarter ellipses on Figures 2 and 3. The orientation of the each of the trace lines identified on the upper and lower surfaces of the core samples were recorded by measuring the angles of these lines with respect to the core axis. Direct measurement of fracture trace line orientations from the two exposed surfaces was not possible. To alleviate this problem, the exposed surfaces of each core sample were photographed using 35 mm colour slide film. The slide images of the exposed surfaces were projected onto 0.2 m long full-scale maps of the upper and lower surfaces of the

core samples. The trace lines of the weathered fractures were then hand drawn from the projected image directly onto the core maps. Figure 4 displays the core sample map prepared for core 3 which was obtained from a interval of 3.8 m to 4.15 m below ground surface along the axis of BH #7. This core sample map shows the trace lines of two intersected fractures, one of each orientation case, that were hand drawn from the slide images of the exposed surfaces of the core. The fracture plane trace line orientations with respect to the core sample axis were easily measured from these maps.

During the fracture mapping, as each core lay horizontally with the top of the sample pointing vertically upwards, a temporary mapping coordinate system $X^m Y^m Z^m$ was defined to lie along the core sample axis. With the origin positioned at ground surface, the Y^m-axis, referred to as the mapping north, was oriented along the axis of the core sample with the down hole direction being positive. The X^m-Y^m plane, referred to as the mapping horizontal plane, was oriented along the core axis perpendicular to the direction of top of the core. The positive Z^m-axis was oriented opposite to the direction of the top of the core. This coordinate system is indicated on Figures 2 and 3.

The following data, as indicated on Figures 2 and 3, was measured directly from the core sample maps: (1) the angle δ_{Fa}^m is the dip angle of the fracture plane with respect to the mapping coordinate system that is apparent in the view that is perpendicular to the upper surface and is measured in a clockwise direction from the top of the core to the trace line of the fracture plane on the upper surface; (2) the angle β_F^m is the bearing of the fracture plane with respect to the mapping coordinate system and is measured in a clockwise direction from the Y^m-axis to the trace line of the fracture plane on the lower surface; and (3) the angle ϕ is defined as the acute angle between the trace line of the fracture plane on the lower surface and the Y^m-axis.

Determination of the In-Situ Fracture Pole Attitude

After mapping the intersected fracture planes and measuring their orientation with respect to the core axis, the bearing and dip of the pole to each fracture plane was determined through the following four step process:

1. Identify the true dip angle δ_F^m of the fracture plane with respect to the mapping coordinate system.
2. Estimate the bearing angle β_P^m, and dip angle δ_P^m of the pole to the fracture plane defined by the vector P^m. In the mapping coordinate system, the vector P^m represents the direction cosines of the pole to the fracture plane.

3. Rotate the mapping horizontal plane, or the X^m-Y^m plane, by the angle δ_{BH} to the orientation of the in-situ horizontal plane. This operation produces a vector P' which represents the direction cosines of the same pole in the $X'Y'Z'$ coordinate system.
4. Rotate the mapping north, now corresponding to the Y'-axis, by the angle β_{BH} to align it with the in-situ north. This produces the direction cosines of the pole to the in-situ orientation of the intersected fracture plane, denoted by the vector P, in the in-situ XYZ coordinate system where the Y-axis now coincides with the in-situ north. The bearing angle β_P and dip angle δ_P of the in-situ pole are then determined from the direction cosines of the vector P.

Unless the bearing angle of the fracture plane β_F^m is equal to 90°, the apparent dip angle δ_{Fa}^m is not the true fracture plane dip with respect to the mapping coordinate system; however, it is possible to determine the true dip angle δ_F^m in the mapping coordinate system with the angles measured from the core maps. The angle δ_F^m can be visualized by taking a view of the upper exposed surface in a direction that is perpendicular to β_F^m. Along the direction of this view as indicated on Figure 3, the length l_1 on Figure 2 would appear as l_2 and the apparent dip angle would now appear as the true dip angle in the mapping coordinate system. The true dip angle δ_F^m can then be calculated from the inverse tangent of the core sample radius divided by the length l_2. The length l_2 is equal to the sine of ϕ multiplied by the length l_1. The length l_1 is equal to the sample radius divided by the tangent of δ_{Fa}^m. Therefore, after several substitutions, the true dip angle in the mapping coordinate system is given by

$$\delta_F^m = \tan^{-1}\left(\tan \delta_{Fa}^m / \sin \phi\right) \qquad (1)$$

For a horizontal (Case II) fracture plane orientation, δ_{Fa}^m is an obtuse angle and (1) provides a negative result equal to the acute angle made between the fracture trace on the upper surface and the top of the sample. In keeping with the established convention for δ_F^m, this result is equal to δ_F^m less 180°. Thus, for a horizontal fracture plane orientation, 180° must be added to the result of (1) to determine δ_F^m. For the remaining steps the treatment of both horizontal and vertical fractures is identical.

In step two, the attitude of the pole to the identified fracture plane is determined by adding 90° to both β_F^m and δ_F^m which gives the bearing angle β_P^m and the dip angle δ_P^m of the pole in the temporary coordinate system. The attitude of the pole described by the vector P^m, was converted to direction cosines as shown in Figure 5. In Figure 5, P^m is assumed to be a unit vector represented by the line $\overline{OP}$. The vector P^m can be expressed in terms of the direction cosines:

$$\cos \alpha_{X^m} = \frac{\overline{OC}}{\overline{OP}} = \overline{OC} = \overline{AB} = \sin \beta_P^m \cdot \overline{OB} = \sin \beta_P^m \cdot \cos \delta_P^m$$

$$\cos \alpha_{Y^m} = \frac{\overline{OA}}{\overline{OP}} = \overline{OA} = \cos \beta_P^m \cdot \overline{OB} = \cos \beta_P^m \cdot \cos \delta_P^m$$

$$\cos \alpha_{Z^m} = \frac{\overline{OF}}{\overline{OP}} = \overline{OF} = \overline{BP} = \sin \delta_P^m$$

Using following relationships:

$$\sin \delta_P^m = \sin\left(\delta_F^m + 90^\circ\right) = \cos \delta_F^m$$

$$\cos \delta_P^m = \cos\left(\delta_F^m + 90^\circ\right) = -\sin \delta_F^m$$

$$\sin \beta_P^m = \sin\left(\beta_F^m + 90^\circ\right) = \cos \beta_F^m$$

$$\cos \beta_P^m = \cos\left(\beta_F^m + 90^\circ\right) = -\sin \beta_F^m$$

the direction cosines of the pole to the identified fracture plane P^m can be expressed as

$$P^m = \begin{Bmatrix} \cos \alpha_{X^m} \\ \cos \alpha_{Y^m} \\ \cos \alpha_{Z^m} \end{Bmatrix} = \begin{Bmatrix} -\sin \delta_F^m \times \cos \beta_F^m \\ \sin \delta_F^m \times \sin \beta_F^m \\ \cos \delta_F^m \end{Bmatrix} \tag{2}$$

Step three consists of multiplying P^m by the matrix representing the rotation of the mapping horizontal plane to the orientation of the in-situ horizontal plane. This involves the rotation of the Y^m-Z^m plane about the X^m-axis in a counter-clockwise direction through the borehole axis dip angle δ_{BH}. The rotation matrix for step three is given by

$$\mathbf{R}_3 = \begin{bmatrix} 1 & 0 & 0 \\ 0 & \cos \delta_{BH} & \sin \delta_{BH} \\ 0 & -\sin \delta_{BH} & \cos \delta_{BH} \end{bmatrix} \tag{3}$$

and the resulting direction cosines of the pole P' in the coordinate system $X'Y'Z'$ are

$$\mathbf{P}' = \mathbf{P}^m \cdot \mathbf{R}_3 = \begin{Bmatrix} \cos \alpha_{X'} \\ \cos \alpha_{Y'} \\ \cos \alpha_{Z'} \end{Bmatrix} = \begin{Bmatrix} \cos \alpha_{X^m} \\ \cos \alpha_{Y^m} \ \cos \delta_{BH} + \cos \alpha_{Z^m} \ \sin \delta_{BH} \\ -\cos \alpha_{Y^m} \ \sin \delta_{BH} + \cos \alpha_{Z^m} \ \cos \delta_{BH} \end{Bmatrix} \tag{4}$$

In step four, the Y'-X' plane is rotated in a counter-clockwise direction about the Z'-axis through the borehole bearing angle β_{BH}. Using the following rotation matrix on P' (5)

$$\mathbf{R}_4 = \begin{bmatrix} 1 & 0 & 0 \\ 0 & \cos \beta_{BH} & \sin \beta_{BH} \\ 0 & -\sin \beta_{BH} & \cos \beta_{BH} \end{bmatrix}$$

yields

$$\mathbf{P} = \mathbf{P}' \cdot \mathbf{R}_4 = \begin{Bmatrix} \cos\alpha_X \\ \cos\alpha_Y \\ \cos\alpha_Z \end{Bmatrix} = \begin{Bmatrix} \cos\alpha_{X'}\ \cos\beta_{BH} + \cos\alpha_{Y'}\ \sin\beta_{BH} \\ -\cos\alpha_{X'}\ \sin\beta_{BH} + \cos\alpha_{Y'}\ \cos\beta_{BH} \\ \cos\alpha_{Z'} \end{Bmatrix} \tag{6}$$

which represents the direction cosines of the pole P in the in-situ XYZ coordinate system. Finally, using the direction cosines of P in (6), the bearing and dip angles of the pole to the in-situ fracture plane orientation can be determined. Referring to Figure 5 and neglecting the superscript m used to denote the temporary mapping coordinate system, the bearing and dip of P are given by

$$\beta_P = \tan^{-1}\left(\cos\alpha_X / \cos\alpha_Y\right) \tag{7}$$

and

$$\delta_P = \left|\tan^{-1}\left(\cos\alpha_Z / \sqrt{\cos\alpha_X{}^2 + \cos\alpha_Y{}^2}\right)\right| \tag{8}$$

The poles to identified fracture planes are presented on a stereographic projection by plotting the poles on a lower hemisphere equal area, or Schmidt, net. The lower hemisphere Schmidt net is configured with the positive Y-axis directed north, the positive X-axis directed east and the positive Z-axis directed upwards out of the net. The use of the inverse tangent in (7) results in angles the range between ±90°. Thus, (7) does not provide a bearing angle in the usual sense, measured clockwise from north. For this reason, the direction cosines α_X and α_Y for P were inspected to determine which quadrant contains the angle resulting from (7). Based on this inspection the angle β_P was corrected by the necessary multiple of 90° to provide a corrected bearing angle β_P^c which, when measured clockwise from north, lies within the same quadrant as β_P. The attitude of the pole to the fracture plane could then be located on the lower hemisphere plot. The corrected bearing angle β_P^c was measured clockwise from north around the circumference of the Schmidt net. The dip angle δ_P was then measured from the outer edge of the plot. The resulting point represents the pole to the observed fracture plane.

Example Fracture Pole Calculation

Table 1 presents the fracture plane orientation data measured from the example core map shown on Figure 4. The results of the fracture pole orientation calculations described in steps 1 through 4 for the two observed fracture planes shown on Figure 4 are presented in Table 2. Table 2(b) indicates the results of adjusting the calculated bearing angle β_P resulting from (7) to provide the corrected bearing angle β_P^c measured clockwise from north on the lower hemisphere plot.

The method developed in this paper to determine the pole to an observed fracture plane can be confirmed graphically using a Schmidt net. Figure 6 presents a graphical determination of the pole for the second fracture plane shown in Figure 4. The procedure begins by plotting the attitude of the borehole on the Schmidt net. The great circle of the lower surface corresponds to the Schmidt net meridian that intersects the borehole attitude. The great circle of the upper surface corresponds to the single line passing through the borehole attitude that bisects the Schmidt net. The great circles of the lower and upper surfaces are shown on Figure 6. The intersection of the apparent dip angle δ_{Fa}^{m} with the upper surface is measured from the borehole attitude along the great circle of the upper surface in a downward direction from the top of the core as the angle is measured on Figures 2(a) and 3(a). The intersection of the bearing angle β_{F}^{m} with the lower surface is measured from the borehole attitude along the great circle of the lower-right quarter from the downhole side of the core axis in an uphole direction as the angle is measured on Figures 2(b) and 3(b). The two intersection points can then be aligned along the common Schmidt net meridian corresponding to the great circle of the intersected fracture plane. The location of the pole to the fracture plane is then determined by measuring a 90° angle along a Schmidt net axis from the mid-point of the fracture plane meridian. The dip angle of the pole δ_{P} is measured along a Schmidt net axis from the circumference of the Schmidt net. The bearing angle of the pole β_{P} is measured clockwise from north around the circumference of the Schmidt net to the plotted location of the pole. The fracture pole bearing and dip angles from the graphical method presented on Figure 6 are the same as those shown in Table 2, thus confirming the developed analytical geometry technique.

Results and Discussion

The calculated poles to 120 discrete fracture planes observed during the core sample analysis are presented on a lower hemisphere equal area projection plot (see Figure 7). The majority of the fracture pole observations lie around the perimeter of the plot indicating that the fracture planes are primarily vertical to sub-vertical. Previous fracture mapping investigations conducted at the Laidlaw site also identified the weathered clay till fractures as being primarily vertical (Klint, 1996; McKay *et al.*, 1993; Ruland *et al.*, 1991; and D'Astous *et al.*, 1989). The observation points that lie near the centre of the plot indicate that some horizontal to sub-horizontal fracture planes were intersected.

A standard method used to analyze the observation points on a polar plot is to calculate the density of points that lie within a counting circle of a given diameter as it is uniformly shifted about the plot (Kamb, 1959). The point density values obtained from this procedure are contoured and these contours are used to identify clusters of fracture pole observations that have similar orientations. Robin and Jowett (1986) developed an algorithm to perform density

contouring and statistical evaluations of orientation data using counting circles and continuous Gaussian weighting functions. The algorithm was applied in this study to analyze the calculated fracture pole data. The contoured equal area projection plot determined using this algorithm is shown on Figure 8. The contoured intervals are shaded to assist in the identification of the peak observation point densities. A list of the statistical parameters determined by the algorithm for the fracture pole densities are shown in the bottom right corner of this figure. The first three parameters are the greatest calculated peak density value (Peak), the peak density value that corresponds to the 99% confidence level (P99) and the peak density value that corresponds to the 95% confidence level. Definitions of the remaining parameters are given in Robin and Jowett (1986).

Three sets of peak densities are evident in the contoured density plot. These are identified as peak density sets 1, 2 and 3 on Figure 9. The peak sets identify a concentration of calculated fracture poles with similar orientations. Each peak set corresponds to a set of fracture planes with orientations that are orthogonal to the orientation of the calculated fracture poles. Having identified these peaks, it is necessary to determine which, if any, are statistically significant. The density values calculated for each peak set are listed in Table 3. Of the three pairs of peaks that make up each peak set, only peak # 1.1, with a density value of 5.66, is above the P95 value of 5.20. Thus, the density of peak #1.1 is statistically significant at a 95% confidence level.

The three sets of peak contour densities for the fracture pole observations indicate the presence of three sets of fracture plane orientations. Corresponding to the density peak labels, the orientation of fracture plane set 1 would be in the east-west direction, the orientation of fracture plane set 2 would be in the northwest-southeast direction, and the orientation of fracture plane set 3 would be in the northeast-southwest direction. Fracture plane sets 2 and 3 are nearly orthogonal to one another. Fracture plane set 1 lies approximately 45° between sets 1 and 3.

A fracture orientation investigation conducted at the Lambton Generating Station also found three fracture plane sets with similar orientations (Vorauer *et al.*, 1986). The three sets were oriented in the northeast-southwest, east-west and southeast-northwest directions. These sets were, however, oriented at approximately 60° angles to one another unlike the three sets observed in this study. At the Laidlaw site, a fracture orientation conducted by McKay *et al.* (1993) identified two orthogonal fracture sets oriented in the east-west and north-south directions. The fracture plane orientations found in this study confirms the presence of the east-west oriented fracture plane set.

To qualify the findings presented in this paper, the bearings of the boreholes from which the calculated fracture pole orientations were determined are plotted on the equal area projection plot shown in Figure 9. It is evident from this figure that there are three groups of borehole bearing angles from which the calculated fracture pole observations were obtained. The three fracture

plane sets identified are, for the most part, orthogonal to these three sets of borehole bearing angles. It would seem that a definite trend in the observed fracture set orientations has been introduced by the bearing angles of the boreholes used to conduct the fracture mapping. For the fracture pole calculation method developed in this study, the orientation of an identified fracture plane can only be determined from the core sample fracture mapping approach if the fracture plane is oriented orthogonally or sub-orthogonally to the bearing of core sample axis. If a fracture plane parallel to the borehole bearing angle was intersected, the ability to identify that fracture plane on the exposed upper or lower surfaces of the core sample is limited.

Summary

The developed method illustrates a framework that can be applied in future studies to increase the amount of fracture orientation information gained from a piezometer network. The method alleviates the need to map fractures on the exposed surfaces of trench excavations. The core sampling technique is an intermediate step easily implemented during piezometer installation. The collected core samples can be removed from the site to be analyzed in a controlled laboratory setting leaving behind a piezometer network where further field experiments can be continued. Although the developed core sampling technique requires certain care to implement, it does not significantly hinder the piezometer installation process. The core sample mapping technique which is critical to this approach can be tedious and time consuming. The identification of intersected fracture planes is also inherently subjective.

The fracture orientation results presented in this study are encouraging. This is the first fracture mapping study conducted within the shallow weathered zone of the clay till deposit found at the Laidlaw site that provides confidence intervals for the preferential fracture plane orientations that were identified. It appears, however, that the fracture plane orientation trends observed in this study could possibly have been introduced by the borehole orientations from which the mapped core samples were obtained. As a result, it can not be assumed that the calculated fracture pole orientations represent a random sample obtained from a parent population of fracture planes with a preferred orientation. Perhaps by obtaining fracture pole observations from a wider range of borehole bearing angles, a more definitive fracture plane orientation data set could be compiled. However, the utility of this methodology has merit and therefore should be explored at other fractured clay till sites.

References

Balfour, D.J., Evaluation of Lateral Solute Migration in Surficial Weathered Clayey Till, M.Sc. Project, University of Waterloo, Waterloo, Ont., Can., 1991.

Bosscher , P.J., and D.E. Connell, Measurement and analysis of jointing properties in fine-grained soils, J. Geotech. Eng, 114(7), 826-843, 1988.

D'Astous, A.Y., W.W. Ruland, J.R.G. Bruce, J.A. Cherry, and R.W. Gillham, Fracture effects in the shallow groundwater zone in weathered Sarnia-area clay, Can. Geotech. J., 26, 43-56, 1989.

Harding, D., An Investigation of the Effective Stress-Permeability Relationship for a Fractured Clay Till Near Sarnia, Ontario, M.Sc. Thesis, University of Waterloo, Waterloo, Ont., Can.,1986.

Harris, S.M., N.R. Thomson, and K.S. Novakowski, Hydraulic characterization of a small clay-till site, in preparation, 1996.

Kamb, W.B., Ice petrofabric observations from Blue Glacier, Washington, in relation to theory and experiments, J. Geophys. Res., 64, 1891-1919, 1959.

Klint, K.E.S., Fractures and depositional features of the St. Joseph Till and upper part of the Black Sale Till at the Laidlaw site, Lambton County, Ontario, Geological Survey of Denmark and Greenland, Report, 1996/9, 39 pp., 1996.

Lau, J.S.O., The determination of true orientations of fractures in rock cores, Can. Geotech. J., 20, 221-227, 1983.

McKay, L.D., J.A. Cherry and R.W. Gillham, Field experiments in a fractured clay till: hydraulic conductivity and fracture aperture, Water Resour. Res., 29(4), 1149-1162, 1993.

Robin, P.-Y.F., and E.C. Jowett, Computerized density contouring and statistical evaluation of orientation data using counting circles and continuous weighting functions, Tectonophysics, 121, 207-223, 1986.

Ruland, W.W., J.A. Cherry, and S. Feenstra, The depth of fractures and active groundwater flow in a clayey till plain in Southwestern Ontario, Ground Water, 29(3), 405-417, 1991.

Vorauer, A.G., D.W. Harding, M.B. Dusseault, and J.A. Cherry, The nature of near-surface fractures in clay tills of Southwestern Ontario, 3rd Canadian Hydrogeological Conference, Intl. Assoc. of Hydrogeologists, Saskatoon. Saskatchewan, April 21-22, 1986.

Acknowledgments

The authors are thankful to C. Jowett and P.-Y. F. Robin for their assistance with the density contouring and statistics associated with the fracture orientation data; and to J.A. Cherry for his constant encouragement and his financial assistance provided from Laidlaw Environmental Services Inc.

Table 1. Borehole attitude and fracture plane mapping data for the fracture planes shown in Figure 4.

Example Fracture Plane	BH #	Borehole Attitude		Core #	Core Depth Interval	Data Measured From Core Map					
						Case I Orientation			Case II Orientation		
		β_{BH}	δ_{BH}			δ_{Fa}^{m}	ϕ	β_{F}^{m}	δ_{Fa}^{m}	ϕ	β_{F}^{m}
1	7	315.6	35	3	3.80 to 4.15	60	75	75			
2	7	315.6	35	3	"				110	80	100

Table 2(a). Pole attitude calculations for the fracture planes shown in Figure 4.

Example Fracture Plane	True dip angle (Step 1) δ_{F}^{m}	Direction Cosines of P^{m} (Step 2)			Direction Cosines of P (Steps 3 & 4)			Calculated Pole Attitude	
		$\cos\alpha_{X^m}$	$\cos\alpha_{Y^m}$	$\cos\alpha_{Z^m}$	$\cos\alpha_{X}$	$\cos\alpha_{Y}$	$\cos\alpha_{Z}$	β_{P} (7)	δ_{P} (8)
1	60.9	-0.226	0.844	0.487	-0.840	0.535	-0.085	-57.5	4.9
2	109.7	0.163	0.927	-0.337	-0.279	0.519	-0.808	-28.3	53.9

Table 2(b). Correction to bearing angle of pole.

Quadant Location of β_P from direction cosines $\cos\alpha_X$ and $\cos\alpha_Y$	β_{P}^{c} Correction Angle	Corrected Pole Bearing Angle β_{P}^{c}
4	360	302.5
4	360	331.7

Table 3. Fracture pole contour density peak values as determined from the Robin and Jowett (1986) algorithm. Peak densities greater than a value of 5.20 are statistically significant at the 95% confidence level.

Identified Density Peak	Calculated Peak Density Value
Peak # 1.1	5.66
Peak # 1.2	4.44
Peak # 2.1	4.63
Peak # 2.2	3.93
Peak # 3.1	4.30
Peak # 3.2	4.56

Post-It™ brand fax transmittal memo 7671 # of pages ▸ 12
To KENT NOWAKOWSKI From N. Thomson
Co. CCIW Co. UofW
Dept. Phone #
Fax # 905-336-4972 Fax #

List of Figures

Figure 1(a).

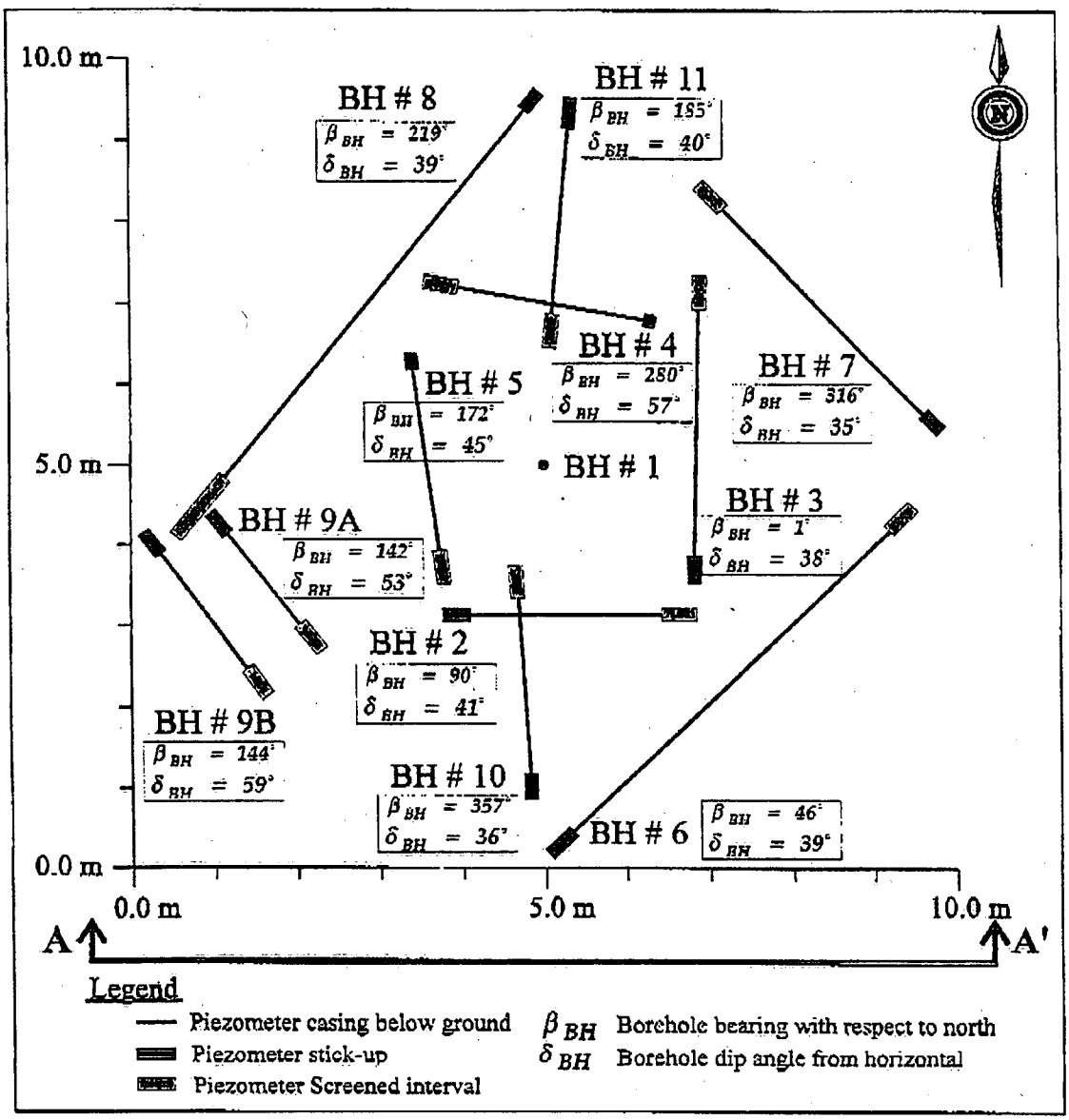
10.0 m
5.0 m
0.0 m
0.0 m
5.0 m
10.0 m
A
A'
BH # 8
β_{BH} = 219°
δ_{BH} = 39°
BH # 11
β_{BH} = 185°
δ_{BH} = 40°
BH # 4
β_{BH} = 280°
δ_{BH} = 57°
BH # 5
β_{BH} = 172°
δ_{BH} = 45°
BH # 7
β_{BH} = 316°
δ_{BH} = 35°
BH # 1
BH # 9A
β_{BH} = 142°
δ_{BH} = 53°
BH # 3
β_{BH} = 1°
δ_{BH} = 38°
BH # 2
β_{BH} = 90°
δ_{BH} = 41°
BH # 9B
β_{BH} = 144°
δ_{BH} = 59°
BH # 10
β_{BH} = 357°
δ_{BH} = 36°
BH # 6
β_{BH} = 46°
δ_{BH} = 39°
N
Legend
Piezometer casing below ground
Piezometer stick-up
Piezometer Screened interval
β_{BH} Borehole bearing with respect to north
δ_{BH} Borehole dip angle from horizontal

Figure 1(b).

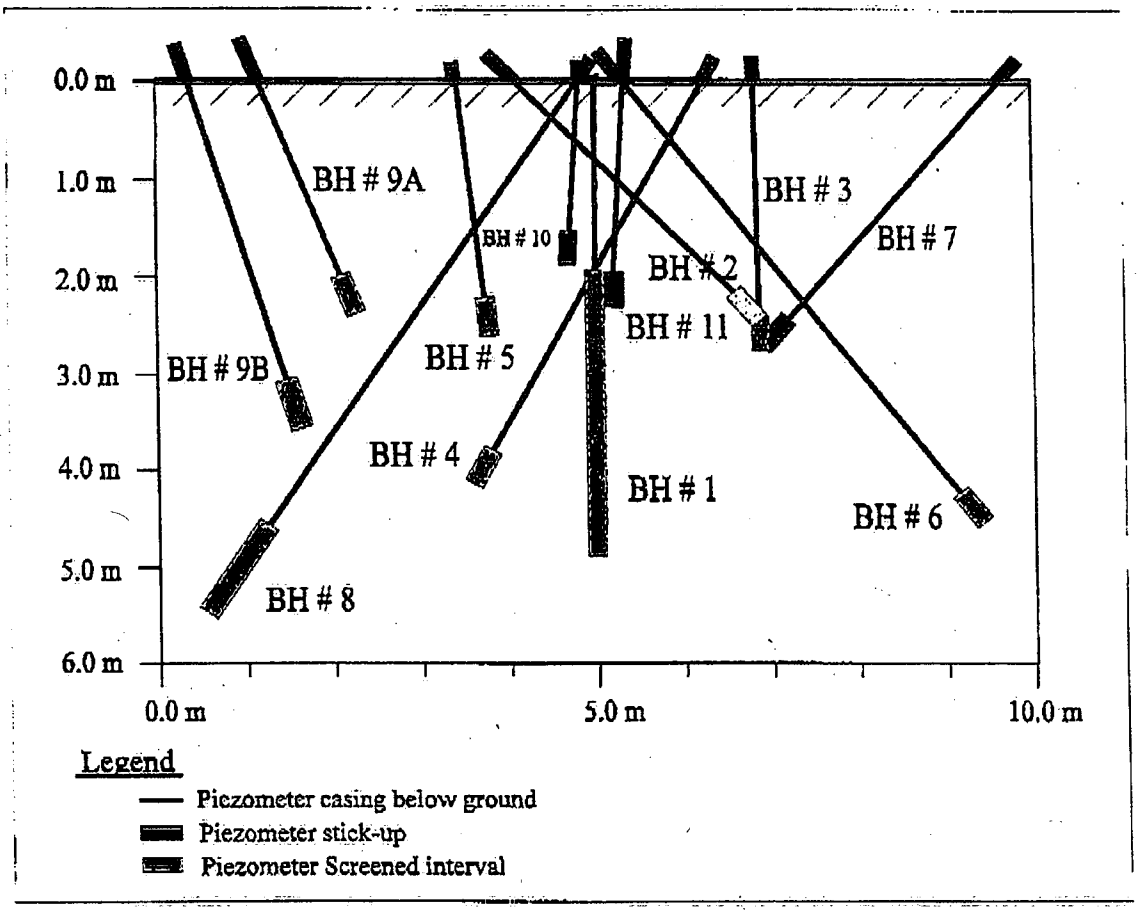
0.0 m
1.0 m
2.0 m
3.0 m
4.0 m
5.0 m
6.0 m
0.0 m
5.0 m
10.0 m
BH # 9A
BH # 10
BH # 3
BH # 7
BH # 2
BH # 11
BH # 9B
BH # 5
BH # 4
BH # 1
BH # 6
BH # 8
Legend
Piezometer casing below ground
Piezometer stick-up
Piezometer Screened interval

Figure 2.

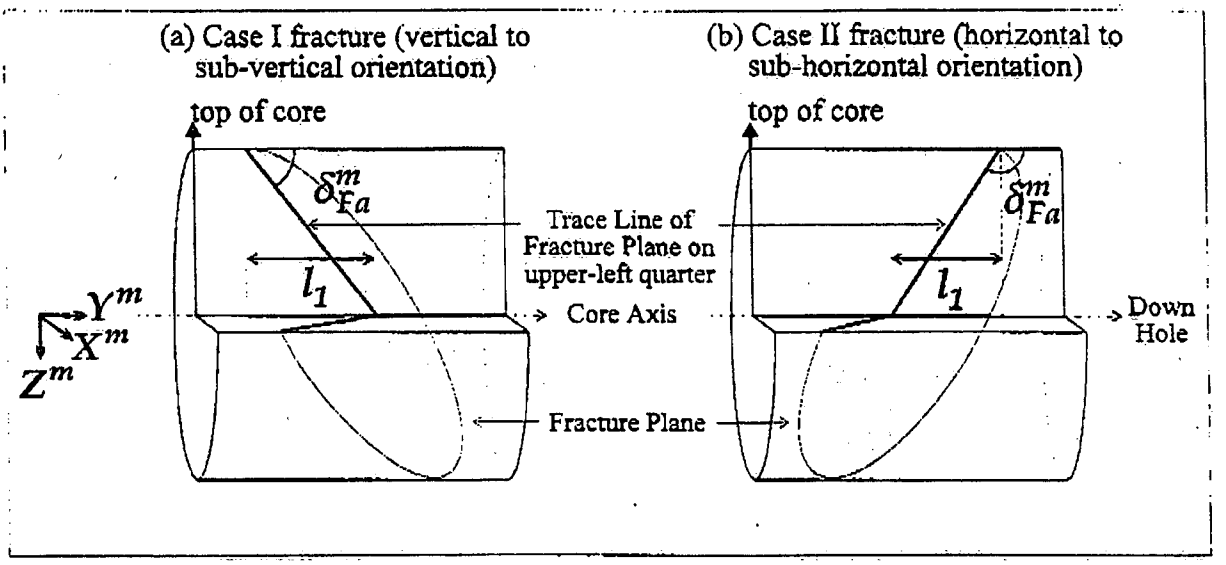

Figure 3.

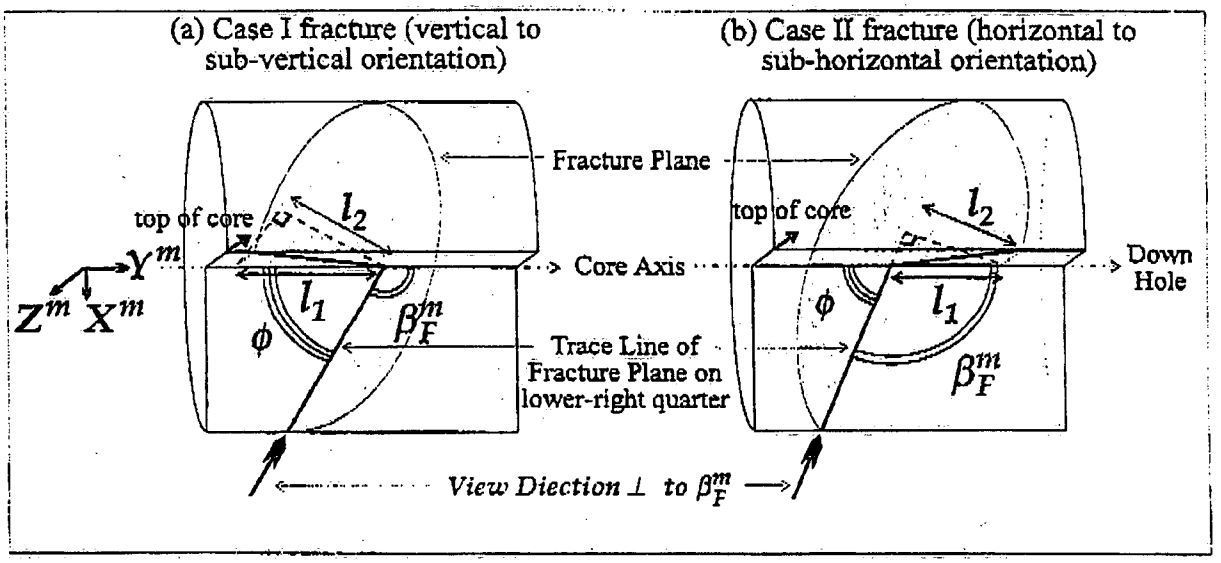

Table 1. Borehole attitude and fracture plane mapping data for the fracture planes shown in Figure 4.

Example Fracture Plane	BH #	Borehole Attitude		Core #	Core Depth Interval	Data Measured From Core Map					
						Case I Orientation			Case II Orientation		
		β_{BH}	δ_{BH}			δ_{Fa}^{m}	ϕ	β_{F}^{m}	δ_{Fa}^{m}	ϕ	β_{F}^{m}
1	7	315.6	35	3	3.80 to 4.15	60	75	75			
2	7	315.6	35	3	"				110	80	100

Table 2(a). Pole attitude calculations for the fracture planes shown in Figure 4.

Example Fracture Plane	True dip angle (Step 1) δ_{F}^{m}	Direction Cosines of P^{m} (Step 2)			Direction Cosines of P (Steps 3 & 4)			Calculated Pole Attitude	
		$cos\alpha_{X^m}$	$cos\alpha_{Y^m}$	$cos\alpha_{Z^m}$	$cos\alpha_{X}$	$cos\alpha_{Y}$	$cos\alpha_{Z}$	β_P (7)	δ_P (8)
1	60.9	-0.226	0.844	0.487	-0.840	0.535	-0.085	-57.5	4.9
2	109.7	0.163	0.927	-0.337	-0.279	0.519	-0.808	-28.3	53.9

Table 2(b). Correction to bearing angle of pole.

Quadant Location of β_P from direction cosines $cos\alpha_X$ and $cos\alpha_Y$	β_P^c Correction Angle	Corrected Pole Bearing Angle β_P^c
4	360	302.5
4	360	331.7

Table 3. Fracture pole contour density peak values as determined from the Robin and Jowett (1986) algorithm. Peak densities greater than a value of 5.20 are statistically significant at the 95% confidence level.

Identified Density Peak	Calculated Peak Density Value
Peak # 1.1	5.66
Peak # 1.2	4.44
Peak # 2.1	4.63
Peak # 2.2	3.93
Peak # 3.1	4.30
Peak # 3.2	4.56

Figure 4.

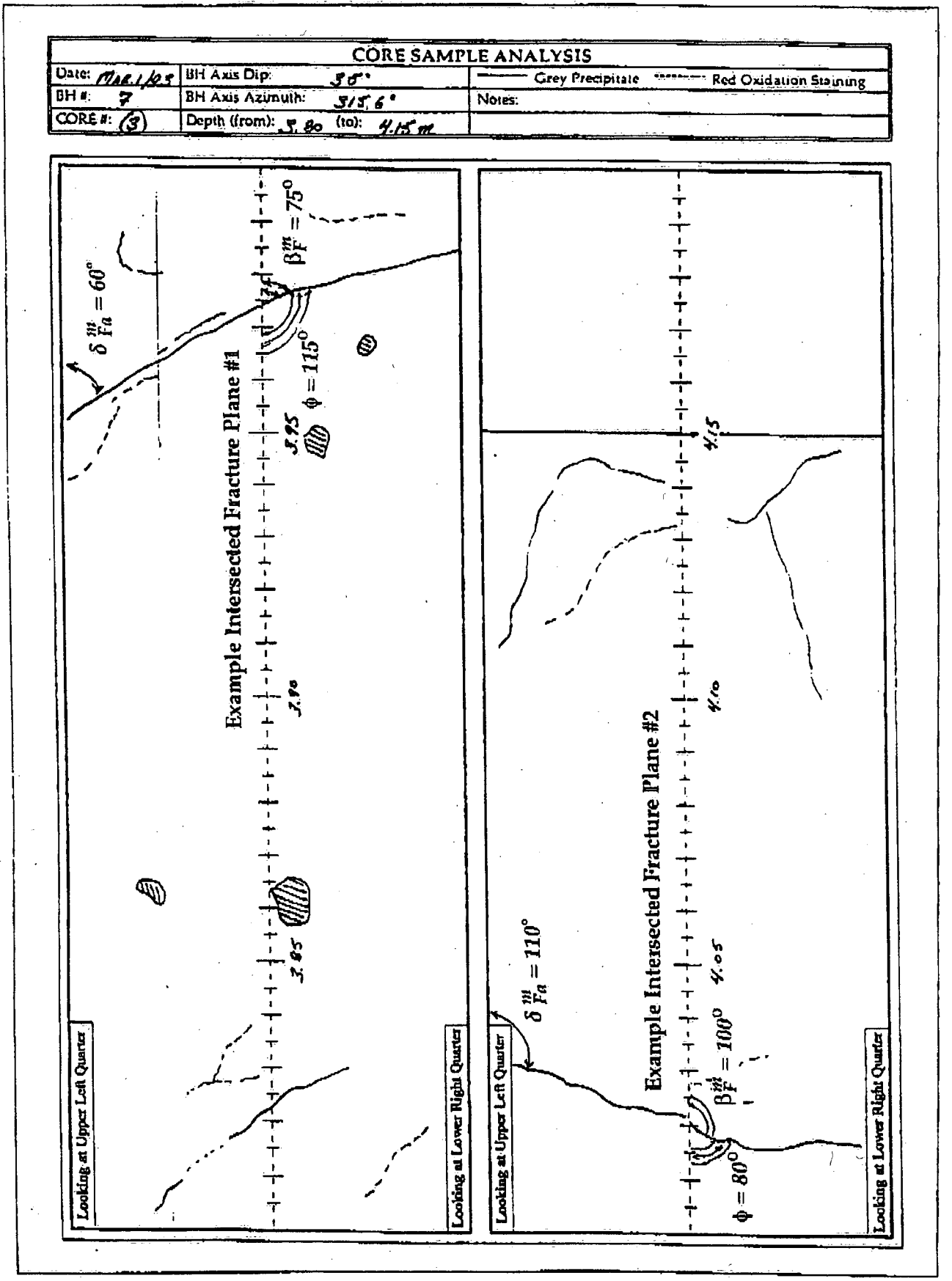
CORE SAMPLE ANALYSIS
Date: Mar. 1/95
BH #: 7
CORE #: (3)
BH Axis Dip: 35°
BH Axis Azimuth: 315.6°
Depth (from): 3.80 (to): 4.15 m
Grey Precipitate
Red Oxidation Staining
Notes:
Example Intersected Fracture Plane #1
$\delta^{m}_{Fa} = 60°$
$\beta^{m}_{F} = 75°$
$\phi = 115°$
3.95
3.90
3.85
Looking at Upper Left Quarter
Looking at Lower Right Quarter
Example Intersected Fracture Plane #2
$\delta^{m}_{Fa} = 110°$
$\beta^{m}_{F} = 100°$
$\phi = 80°$
4.15
4.10
4.05
Looking at Upper Left Quarter
Looking at Lower Right Quarter

Figure 5.

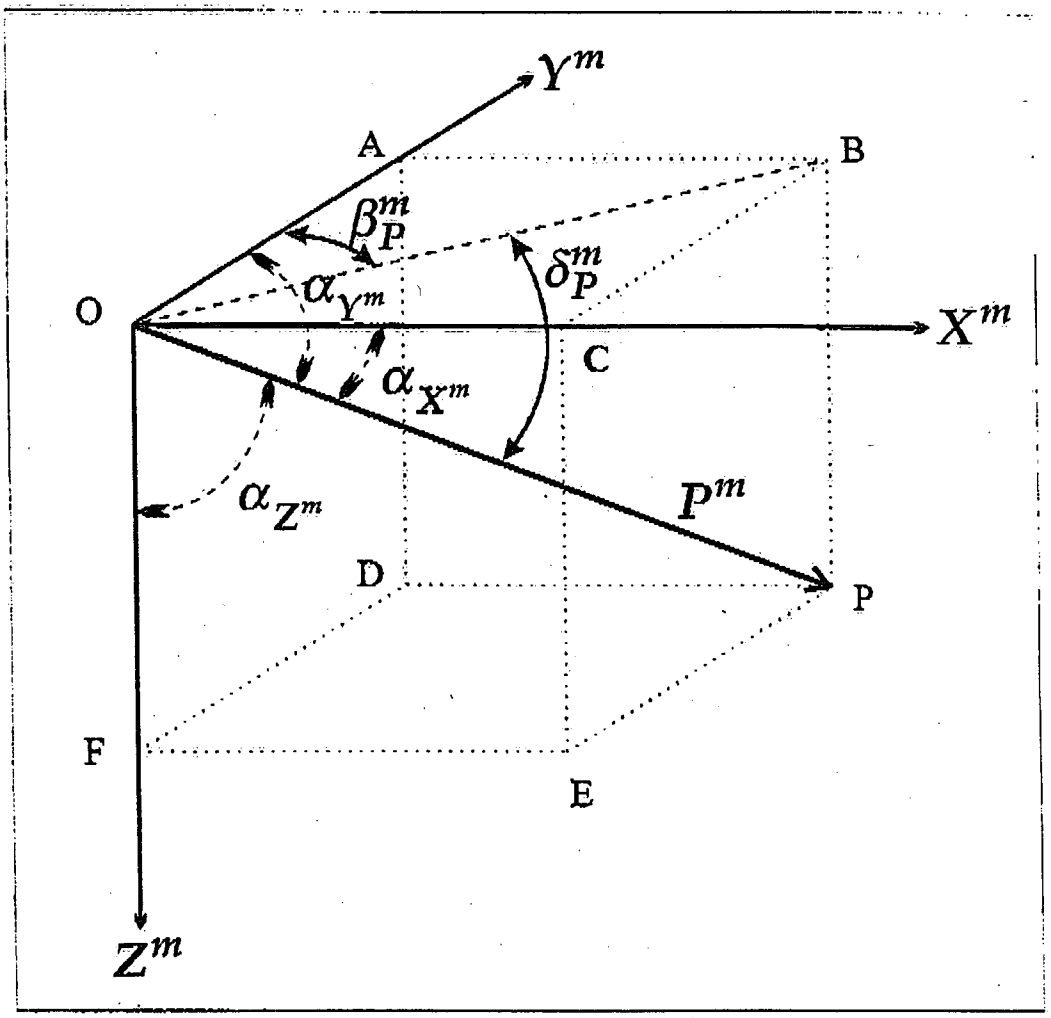
Y^m
A
B
β_P^m
δ_P^m
α_{Y^m}
O
X^m
C
α_{X^m}
α_{Z^m}
P^m
D
P
F
E
Z^m

Figure 6.

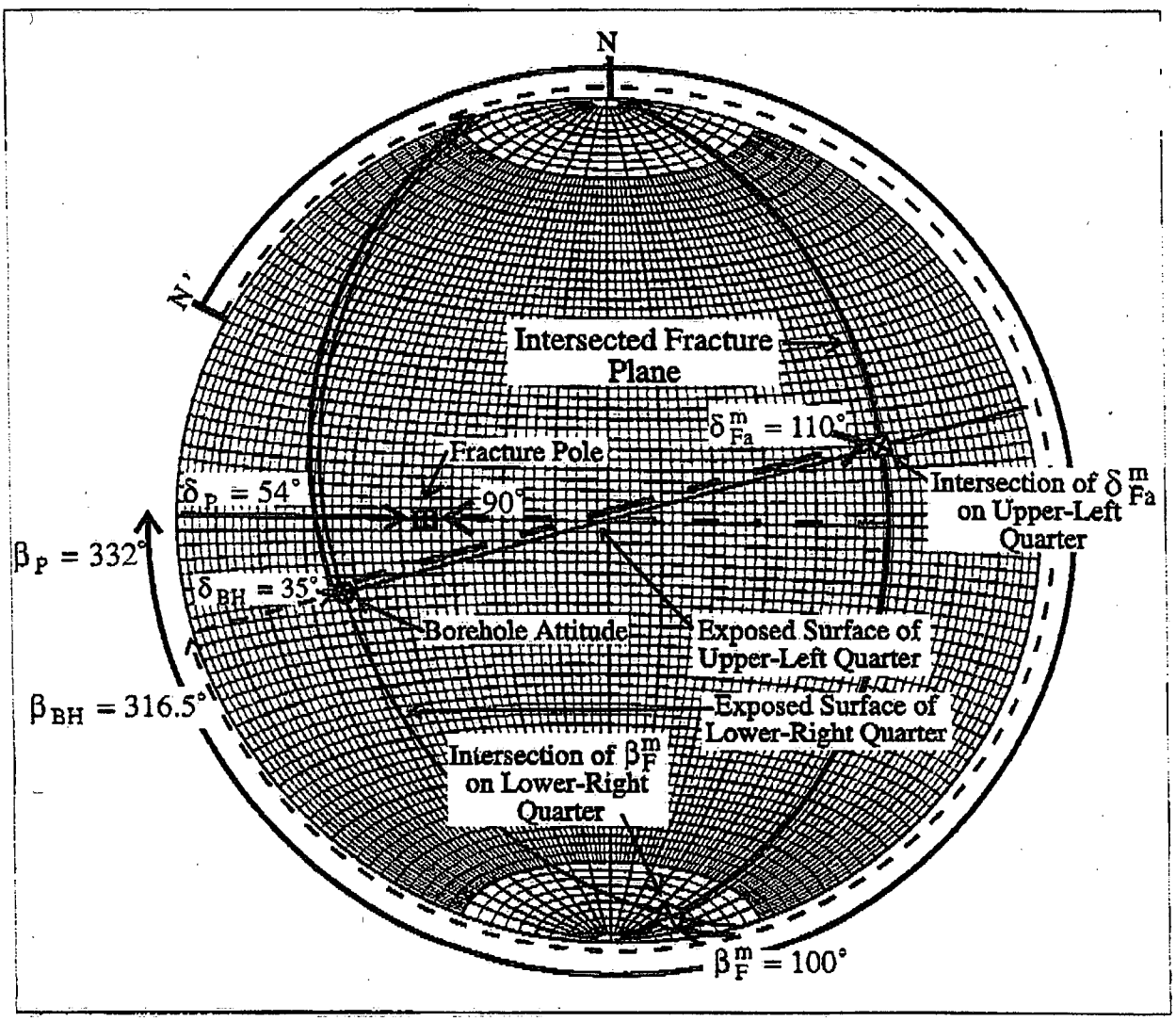
N
N'
Intersected Fracture Plane
$\delta^{m}_{Fa} = 110°$
Fracture Pole
$\delta_P = 54°$
90°
$\beta_P = 332°$
$\delta_{BH} = 35°$
Borehole Attitude
Exposed Surface of Upper-Left Quarter
Intersection of δ^{m}_{Fa} on Upper-Left Quarter
$\beta_{BH} = 316.5°$
Exposed Surface of Lower-Right Quarter
Intersection of β^{m}_{F} on Lower-Right Quarter
$\beta^{m}_{F} = 100°$

Figure 7.

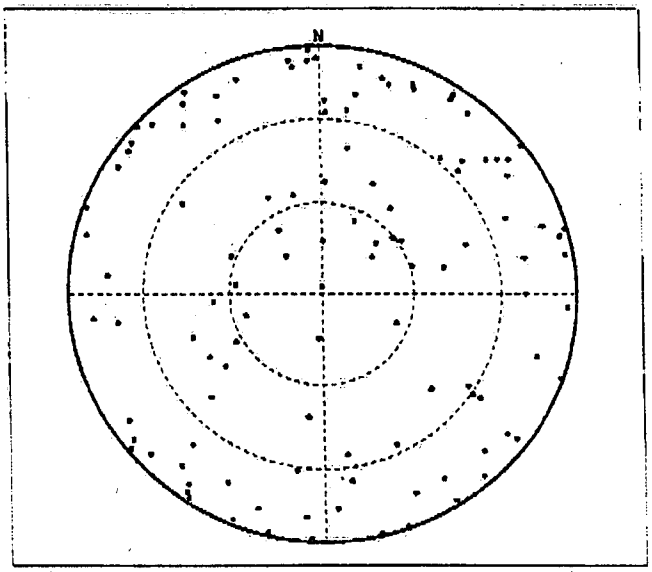

Figure 8.

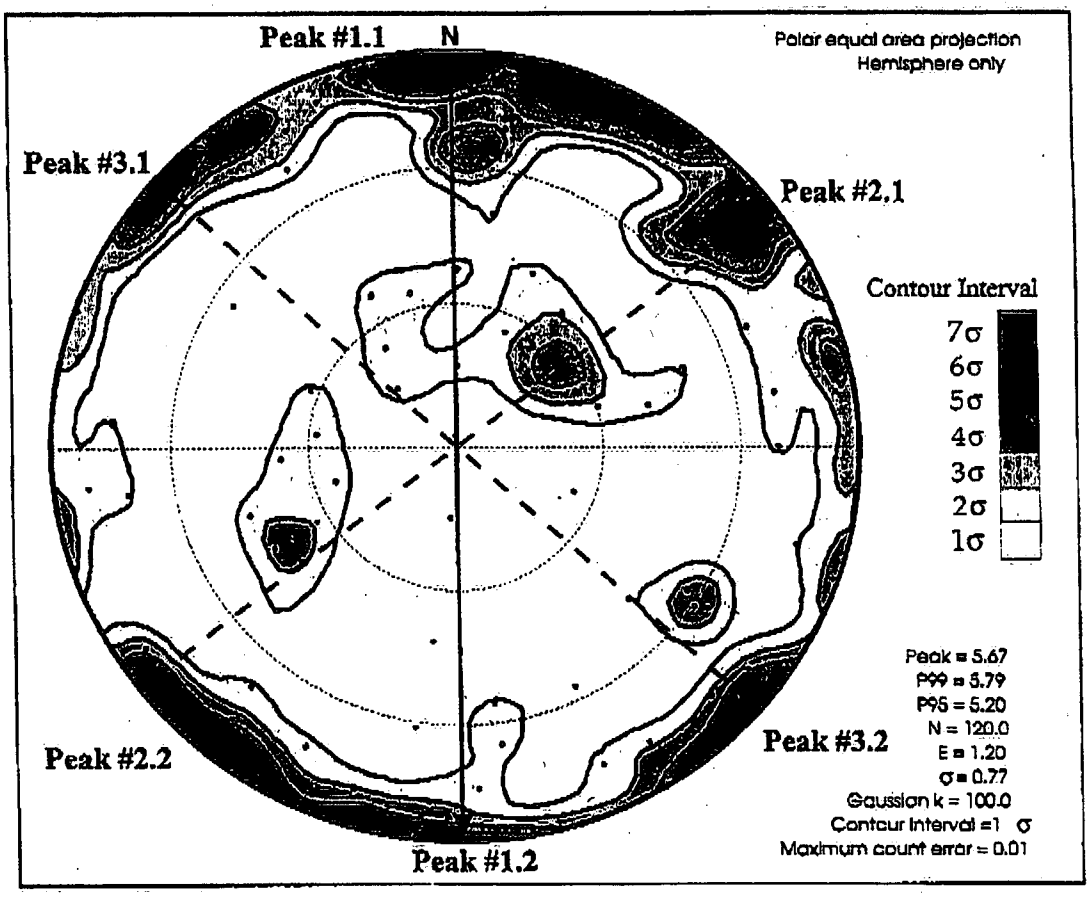
Peak #1.1
N
Polar equal area projection
Hemisphere only
Peak #3.1
Peak #2.1
Contour Interval
7σ
6σ
5σ
4σ
3σ
2σ
1σ
Peak = 5.67
P99 = 5.79
P95 = 5.20
N = 120.0
E = 1.20
σ = 0.77
Gaussian k = 100.0
Contour Interval =1 σ
Maximum count error = 0.01
Peak #2.2
Peak #3.2
Peak #1.2

Figure 9.

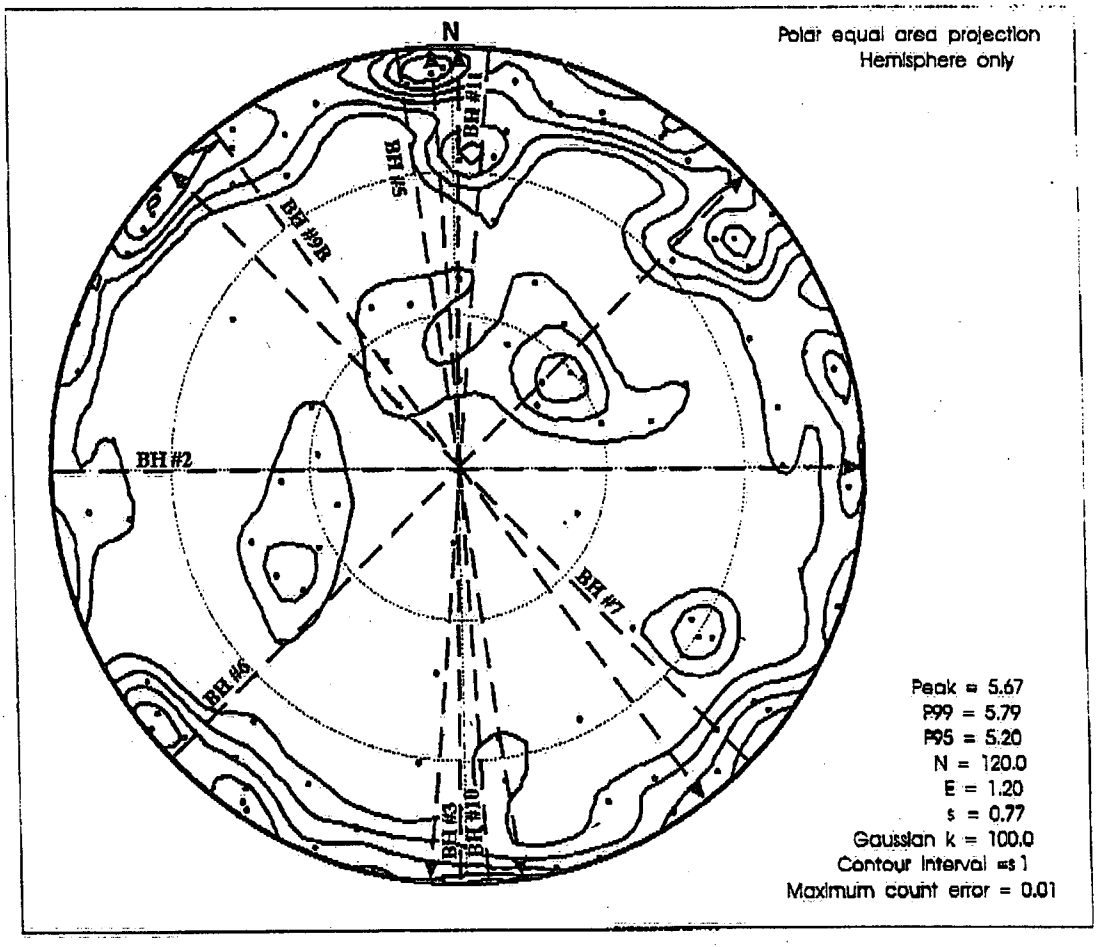
N
Polar equal area projection
Hemisphere only
BH #1
BH #5
BH #9R
BH #2
BH #7
BH #6
BH #3
BH #10
Peak = 5.67
P99 = 5.79
P95 = 5.20
N = 120.0
E = 1.20
s = 0.77
Gaussian k = 100.0
Contour interval = 1
Maximum count error = 0.01

Environment Canada Environnement Canada

Canada

Canada Centre for Inland Waters
P.O. Box 5050
867 Lakeshore Road
Burlington, Ontario
L7R 4A6 Canada

National Hydrology Research Centre
11 Innovation Boulevard
Saskatoon, Saskatchewan
S7N 3H5 Canada

St. Lawrence Centre
105 McGill Street
Montreal, Quebec
H2Y 2E7 Canada

Place Vincent Massey
351 St. Joseph Boulevard
Gatineau, Quebec
K1A 0H3 Canada

Centre canadien des eaux intérieures
Case postale 5050
867, chemin Lakeshore
Burlington (Ontario)
L7R 4A6 Canada

Centre national de recherche en hydrologie
11, boul. Innovation
Saskatoon (Saskatchewan)
S7N 3H5 Canada

Centre Saint-Laurent
105, rue McGill
Montréal (Québec)
H2Y 2E7 Canada

Place Vincent-Massey
351 boul. St-Joseph
Gatineau (Québec)
K1A 0H3 Canada